RESEARCH ARTICLE

Numerical optimization of hydrothermal liquefaction process for the production of bio-oil and bio-char from *Citrus maxima* peel waste and product characterization

Afzal Hussain[1] · Sanjay Kumar[2] · Fohad Mabood Husain[3] · Vinod Kumar[2,4] · Mikhail S. Vlaskin[5] · Mohamed F. Alajmi[1]

Abstract

This research study aims to potential utilization of *Citrus maxima* peel waste and optimize the hydrothermal liquefaction process for the production of bio-oil (BO) and bio-char (BC). The effect of several HTL processing variables on BO yield (%) and BC yield (%), including temperature, retention period, and slurry concentration, has been examined using central composite design (CCD) (a three-level three-factor design). The optimized values of HTL process variables were found to be 240 °C (temperature), 52 min (retention time), and 7% (slurry concentration) and the corresponding responses were 5.794% (BO yield) and 29.450% (BC yield). The values obtained from the RSM-CCD model as the predicted values agreed with the experimental values (5.93% and 30.14%). Further the BO and BC obtained under optimized conditions and CPP were analyzed to identify the variations by ^{1}H-NMR, GC–MS, FT-IR, and CHNO-S.

Keywords Response surface · Central composite design · Pomelo peel · Nuclear magnetic resonance · Design expert · Response surface

Introduction

Globally, the population is increasing, leading to the reduction in the non-renewable resources for societies and altering the sustainable food supply system. Population growth relates to the increasing worldwide request for energy and consumption of fossil fuels. Fossil fuels currently provide 84 percent of the global energy needs; nevertheless, it is predicted that this consumption will rise by 50 percent in the upcoming years (Shafiee and Topal 2009). It is necessary to create low-cost, environmentally friendly, biodegradable, and less hazardous renewable energy sources that minimize or eliminate particulate emissions, carbon monoxide, and total hydrocarbons (Xue et al. 2011; Naruka et al. 2019; Kumar et al. 2019a, b; Kumar et al. 2019a, b; Arora et al. 2020).

Many efforts have been made in order to produce second-generation bio-fuel, such as fuel of ethanol from non-consumable waste generated from the fruits of a citrus family because they consist of soluble saccharides, i.e., monosaccharides or disaccharides, for example, glucose, fructose, and sucrose, and lignin, insoluble polysaccharides, for example, pectin, hemicellulose, and cellulose (Ting and Deszyck 1961). These chemical compositions of citrus wastes have the potential to produce bio-fuels and other chemicals that are sugar-based (Ángel Siles López and Thompson 2010; Pourbafrani et al. 2013). The *Citrus maxima*, known as the pomelo, is mainly grown in various Asian nations. Many people eat pomelo fruit either fresh in raw form or in liquid form as juice. Pomelo peels make

---

Responsible Editor: Ta Yeong Wu

✉ Sanjay Kumar
  mr.sanju4u@gmail.com

  Afzal Hussain
  afhussain@ksu.edu.sa

[1] Department of Pharmacognosy, College of Pharmacy, King Saud University, PO Box 2457, 11451 Riyadh, Saudi Arabia

[2] Department of Food Science and Technology, Graphic Era (Deemed to Be University), Dehradun, Uttarakhand 248002, India

[3] Department of Food Science and Nutrition, College of Food and Agriculture Sciences, King Saud University, Riyadh 11451, Kingdom of Saudi Arabia

[4] Peoples' Friendship, University of Russia, (RUDN University), Moscow 117198, Russian Federation

[5] Joint Institute for High Temperatures of the Russian Academy of Sciences, 13/2 Izhorskaya St, Moscow 125412, Russian Federation

up roughly 45% of the fruit's weight and are frequently disposed of as biological waste (Chen et al. 2020a, b). These wastes contain bio-active substances like flavonoids, pectin, essential oils, and cellulose (Methacanon et al. 2014; Huang et al. 2014). The main constituents of wet pomelo waste are water, carbohydrate, lipids (mainly D-limonene), and bio-active substances. Investigators find more feasible, economical, and systematic plans to pomelo peel waste and recover the value-added products like pectin, essential oils (EOs), and functional food ingredients (Tocmo et al. 2020). This organic waste can be processed using the hydrothermal liquefaction (HTL) method to create bio-ethanol. The HTL process comprises hydrolysis reactions; due to increased temperature, dehydration, decarboxylation reactions, reaction time, and pressure, the HTL process decreases the oxygen concentration of the biomass to approximately 10% in the bio-crude, which may be employed to maximize conversion yields. After completion of the process, hydrothermal liquefaction generates four products: an aqueous phase, bio-crude oil, solid phase, and a stream of gas, which depends on the conditions of the reaction (e.g., temperature and time). HTL can be considered as the most efficient technique for producing different products; for example, the solid product may be used as activated carbon-based compounds for energy and environmental applications. Furthermore, greater BO yield was obtained in HTL compared to other technologies and thus has the potential to be used as transportation fuels. Additionally, direct aqueous phase use includes anaerobic digestion, catalytic hydrothermal gasification, or algal growth. HTL-derived bio-crude can be used to replace fossil fuels. Moreover, unlike other technologies such as pyrolysis, HTL does not require drying; therefore, wet feedstock may be liquefied directly, significantly reducing process operating costs. Nonetheless, this shows that the HTL method not only has high energy efficiency but also may deliver significant environmental benefits (Gururani et al. 2022).

HTL promotes better sustainability by simultaneously remediating food waste which is the potential feedstock source for renewable energy production. However, the selection of food waste is critical due to the variable impacts on HTL yields that are influenced by protein, carbohydrate, and fat composition. Several authors have reported on the effect of feedstock composition and reaction circumstances on the various HTL products; for instance, (Chen et al. 2020a, b) used a two-step approach for producing bio-oil from pineapple peel, banana peel, and watermelon peel employing an alkaline pre-treatment process followed by a HTL process. The optimal combination of the four parameters (pre-treatment temperature and time, liquefaction temperature, and holding time) results in a 45.8% improvement in bio-oil. According to the findings of this study, alkaline pre-treatment is favorable

for cleaving chemical bonds in carbohydrate or lignin, hence boosting depolymerization processes in the subsequent HTL process (Chen et al. 2020a, b). This also showed that a greater pre-treatment temperature might hasten the breakdown of the intermolecular framework, yielding more energy at a lower liquefaction temperature (Mazaheri et al. 2013; Li et al. 2015). For example, bagasse, fruit peels, and wood material generally prefer lower HTL temperatures (about 300 °C) (Long et al. 2016) since greater liquefaction temperatures result in the repolymerization of unsaturated products and radicals.

Therefore, the present investigation focuses on producing the production of BO from CPP through the hydrothermal liquefaction (HTL) process. Reaction time, temperature, and slurry concentration were considered as the optimum HTL conditions to get the maximum yield of BO from CPP, based on the experimental design that was systematically studied. The characteristics of the BO and BC were examined with the help of GC–MS, FT-IR (BC), and ^{1}H-NMR. Until now, no work has been done on the optimization-based experimental design for *Citrus maxima* peel powder (CPP) and its evaluation. In this investigation, an approach was made to provide a far-reaching understanding of the HTL and optimization-based experimental design behavior of fruit waste.

Materials and methods

Material and chemical

Mature *Citrus maxima* fruit of fine quality was purchased from the local market of Dehradun, Uttarakhand, India. The fruit was peeled off, and the peel was cut into small thin strips, and dried in a mechanical dryer at 50 °C for 10–12 h. For subsequent investigation, the dried peel was ground into a powder and kept at room temperature in an airtight container. Dichloromethane to rinse the bio-reactor and extraction of the BO was of analytical grade and acquired from HiMedia, India.

Experimental design and hydrothermal liquefaction

A total of 20 experiments were designed for RSM (response surface methodology) utilizing Design Expert 13.0.1 version (Stat-Ease Inc., Minneapolis, USA). Central composite design (CCD) with three independent process variables, i.e., temperature (°C), retention time (min), and slurry concentration for hydrothermal liquefaction, and two dependent variables, i.e., BO yield (%) and BC (%), were agreed on to design the experiments (Table 1). The CCD comprises $2n$ axial and $2n$ factorial runs and central point runs. The total number of an experimental run (*N*) under CCD was obtained by using Eq. (1) given by Sadhukhan et al. (2016).

Table 1 Experimental design with coded and actual values

Coded value	Temperature (°C)	Retention time (min)	Solid to solvent ratio (%)
−1.682	220	20	5
−1	240	28	7
0	270	40	10
1	300	52	13
1.682	320	60	15

Total number of experiments

$$(N) = 2^n + 2n + C_0, \tag{1}$$

where n is an independent variable and C_0 is the center point.

Three basic steps were involved for the optimization of process parameters, i.e., experimental design, coefficient estimation, and model adequacy inspection. Six central points are included in the experimental design to evaluate the error, lack of fit of regression equations, and a sum of squares. To fit the mathematical equation (Eq. (2)), a second-order model was used.

$$Y = \beta_0 + \sum_{i=1}^{3} \beta_j X_i + \sum_{j=1}^{2} \sum_{j=i+1}^{3} \beta_{ij} X_i X_j + \sum_{j=1}^{3} \beta_{ij} X_i^2, \tag{2}$$

where Y is the response; β_0, β_{ii}, and β_{ij} are the coefficients; X_i and X_j are the independent variables ($i = 1,2,……n$ and $j = 1,2,……n$); and X_i and X_j can be calculated from Eq. (3).

$$X_i = \frac{2X_{i-(X_{iHv}-X_{iLv})}}{(X_{iHv} - X_{iLv})} \tag{3}$$

where X_i is the coded variable ($i = 1, 2, 3$) and X_{iHv} and X_{iLv} are the higher and the lower levels of X_i.

Analysis of variance (ANOVA) was used to examine the statistical significance and analyze the interactions of independent process variables that were statistically significant and relative. The model's suitability was quantified by the coefficient of determination (R^2), Fisher's value, adjusted R^2, and lack of fit (LOF) and determined by using Eqs. (4), (5), and (6).

$$R^2 = 1 - [\frac{SS_{Residual error}}{SS_{model} - SS_{Residual}}] \tag{4}$$

$$R^2_{Adj} = 1 - \frac{(N-1)}{(N-P)} \times (1 - R^2) \tag{5}$$

$$F = \frac{MS_{Regression}}{MS_{Residual}} \tag{6}$$

where SS is the sum of square, N is the number of observations, and P is the independent variable (Khuri and Cornell 1987).

Hydrothermal liquefaction of CPP was performed in a 25-mL inner volume, stainless steel (SS-316) reactor. The retention time was counted immediately as the reactor achieved the desired temperature. As the reaction was completed, the reactor cooled down immediately. A vacuum filter separated the water and solid phase; gas was vented off into the air. The solid phase and reactor was rinsed 3–4 times with dichloromethane and dried overnight in a hot air oven at 100 ± 2 °C to obtain the dried solid, i.e., BC. A separating funnel liquid phase with dichloromethane was separated into dichloromethane soluble and aqueous phase insoluble fraction. A rotary evaporator was used to evaporate dichloromethane at 40 °C to obtain the BO. The yield of BO and BC was calculated using Eqs. (7) and (8).

$$BO\ yield\ (\%) = \frac{W_{do}}{W_s} \times 100 \tag{7}$$

$$BC\ yield\ (\%) = \frac{W_{ds}}{W_s} \times 100 \tag{8}$$

where W_{do}, W_{ds}, and W_s are the dry bio-oil, dry solid, and sample weight, respectively.

Instrumental analysis of product

The CHNS Analyzer (Flash 2000 Series, Thermo Scientific) was used to analyze the C, H, N, and S in BC and CPP. The oxygen content was determined by different methods.

A modified method of Kumar et al. (2019a, b) was adopted to analyze the chemical composition of BO using gas chromatography-mass spectrometry (CLARUS SQ8S, PerkinElmer). Briefly, the Agilent VF-5 ms column was used for GC–MS analysis with helium as the carrier gas flowing at a rate of 1 mL/min. The BO was diluted in dichloromethane (DCM) 100 times and purified via PTFE membrane filters (0.2 μm) before injection. One-microliter injection volume and 300 °C injector temperature were employed at a split ratio of 1:10. The column temperature was kept for 2 min at 80 °C before accelerating at a rate of 8 °C/min to 140 °C and then to 280 °C at 4 °C/min for 2 min. The mass spectrometer was programmed with a scanning range of 50 to 1000 m/z and an ionizing voltage of 70 eV. The chemical composition of the

samples was determined by matching the sample spectra to the electron impact mass spectrum from the NIST Database.

The ^{1}H NMR spectra of BO were recorded using the 400-MHz Fourier transform-nuclear magnetic resonance (Bruker Advance-II), and the spectra were integrated again using the functional group outlined by Mullen et al. (2009). Fourier transform infrared spectroscopy (Frontier FT-IR/FIR, Perkin-Elmer) is utilized for identifying the functional groups of CPP and BC along the range of scanning wavelengths from 500 to 4000 cm^{-1}.

Results and discussion

Elemental analysis

Table S1 represents the proximate and elemental analysis of CPP and Table S2 represents the elemental analysis of BC and BO.

Second-order regression models and statistical analysis/central composite design studies

The experimental results are displayed in Table 2. Table 2 depicts that the yield of BO varied from 2.8 to 6.2%, whereas the yield of BC varied from 17.0 to 48.5%. The higher yield of BO was observed at the process parameters, 240 °C

temperature, 52-min retention time, and 7% slurry concentration ratio while the low BO yield was observed at 300 °C, 52 min, and 13%, as seen in the results (Table 2).

ANOVA (analysis of variance) was utilized to know the model's effectiveness. From Table 3, it was observed that the coefficients of determination, i.e., R^2 and adjusted R^2, were 0.8651, 0.7437 and 0.9023, 0.8144 for BO and BC, respectively. The R^2 indicates the relationship strength between model and the process variables and ranges between 0 and 100% scale. Simply we can say that the higher the R^2, the more variation is explained by designed process variables and hence better is the model. As indicated in Table 3, the model of BO and BC yield was determined to be highly significant ($p < 0.01$) F values for both responses were significant, whereas not significant for lack of fit. The lower values of pure error mean square of the model and standard deviation indicate that the experimental data are verifiable. The second-order regression model equations for the responses BO yield and BC yield, i.e., (R_1) and (R_2) in actual factors terms, are given in Eqs. (9) and (10).

BO yield

$$(R_1) = 47.64492 - 0.36272X_1 + 0.64333X_2 - 1.35513X_3 - 2.95139e^{-3}X_1X_2$$
$$+ 1.25e^{-3}X_1X_3 + 7.29167e^{-3}X_2X_3 \tag{9}$$
$$+ 8.53064e^{-3}X_1{}^2 + 9.56652e^{-4}X_2{}^2 + 0.033306X_3{}^2$$

Table 2 CCD arrangement for variables and their response (BO yield and BC yield)

Standard no	Run no	X_1 (°C)	X_2 (min)	X_3 (%)	BO yield (%)	BC yield (%)
1	5	240	28	7	4.8	33.5
2	11	300	28	7	5.6	27.8
3	8	240	52	7	6.2*	30.7
4	13	300	52	7	2.9	22.3
5	1	240	28	13	3.2	48.5*
6	19	300	28	13	4.6	28.1
7	12	240	52	13	5.8	30.5
8	4	300	52	13	2.8**	17**
9	18	220	40	10	5.3	33.6
10	3	320	40	10	5.9	17.6
11	10	270	20	10	3.9	33.6
12	17	270	60	10	3.8	23
13	6	270	40	5	4.1	29.5
14	14	270	40	15	4.5	27.2
15	16	270	40	10	2.9	29.5
16	7	270	40	10	3.2	25.4
17	15	270	40	10	3.5	25.1
18	9	270	40	10	3.3	28.9
19	2	270	40	10	3.3	29.5
20	20	270	40	10	3.9	24.2

X_1 temperature, X_2 retention time, X_3 slurry concentration.

**, *Lowest and highest values

Table 3 ANOVA for the effects of variables on response BO yield and BC yield

Source	BO yield					BC yield					Remark
	Sum of squares	df	Mean square	F value	p-value Prob $> F$	Sum of squares	df	Mean square	F value	p-value Prob $> F$	
Model	19.91	9	2.21	7.13	0.0025	766.75	9	85.19	10.26	0.0006	S
X_1—temperature	0.71	1	0.71	2.28	0.1617	411.28	1	411.28	49.55	<0.0001	
X_2—retention time	0.033	1	0.033	0.11	0.7519	223.70	1	223.70	26.95	0.0004	
X_3—slurry concentration (w/v)	0.44	1	0.44	1.41	0.2630	2.63	1	2.63	0.32	0.5862	
$X_1 X_2$	9.03	1	9.03	29.09	0.0003	2.21	1	2.21	0.27	0.6175	
$X_1 X_3$	0.10	1	0.10	0.33	0.5805	49.00	1	49.00	5.90	0.0355	
$X_2 X_3$	0.55	1	0.55	1.78	0.2123	54.08	1	54.08	6.52	0.0287	
X_1^2	8.27	1	8.27	26.64	0.0004	0.011	1	0.011	1.314E−003	0.9718	
X_2^2	0.27	1	0.27	0.86	0.3762	12.50	1	12.50	1.51	0.2478	
X_3^2	1.26	1	1.26	4.06	0.0716	12.99	1	12.99	1.56	0.2395	
Residual	3.10	10	0.31			83.00	10	8.30			
Lack of fit	2.55	5	0.51	4.59	0.0598	52.94	5	10.59	1.76	0.2748	NS
Pure error	0.56	5	0.11			30.06	5	6.01			
Cor total	23.02	19				849.76	19				
R^2	0.8651					0.9023					
Adjusted R^2	0.7437					0.8144					
Standard deviation	0.56					2.88					

S (significant), *NS* (not significant)

BC yield

$$(R_{12}) = 20.18252 + 0.049789X_1 - 0.53456X_2 + 8.32257X_3$$
$$+ 1.45833e^{-3}X_1X_2 - 0.027500X_1X_3 - 0.072222X_2X_3 - 3.09798e^{-5}X_1^2 \quad (10)$$
$$+ 6.55638e^{-3}X_2^2 + 0.10690X_3^2$$

where X_1, X_2, and X_3 represent the temperature, retention time, and slurry concentration, respectively.

Interaction of independent process variables on responses

Temperature, retention time, and slurry concentration ratio are crucial for the process of liquefaction and significantly affect the BO and BC yields (Zang et al. 2019; Acharya et al. 2022; Divyabharathi and Subramanian 2022). Figure 1 (a), (b), (c), (d), (e), and (f) depict the three-dimensional response surface plots for the impact of independent process variables, temperature, retention time, and solid to the concentration of slurry and their interactive effect on BC and BO yields, respectively.

The interaction between the retention time and temperature on BO yield at constant slurry concentration is depicted in Fig. 1(a). It can be seen that the BO yield increased with an increase in temperature and retention time. This result is in agreement with preceding studies of fresh lemon peel hydrothermal liquefaction (Zang et al. 2019; Jiang and Savage 2017).

The interaction between slurry content and temperature and BO yield at constant retention time is shown in Fig. 1(b). It can be observed that BO yield increased with slurry concentration increases and decreased as the temperature rises with respect to slurry concentration (Gai et al. 2015; Kumar et al. 2018). Figure 1(c) demonstrates slurry concentration and retention time's interactive effect on BO yield at a constant temperature. It was shown that BO yield increased with slurry concentration and retention time increased.

This increase in BO yield can be due to the hydrolysis and breaking of CPP, and the formation of molecules of lower weight (Changi et al. 2015). However, the BO could further break down into gaseous compounds at higher temperatures, reducing the amount of BO produced (Kumar et al. 2018). The interaction between temperature and retention period on BO yield at constant slurry content is shown in Fig. 1(d). It should be observed that as the temperature and retention period increased, the BC yield reduced. The interaction between slurry content and temperature and BO yield at constant retention time is depicted in Fig. 1(e). Increasing temperature apparently caused a decrease in BC production while decreasing with increased slurry concentration. Figure 1(f) demonstrates the interactive effect of slurry concentration and retention time on BO yield with respect to a constant temperature. It can be seen that BC yield decreases as the retention time increases.
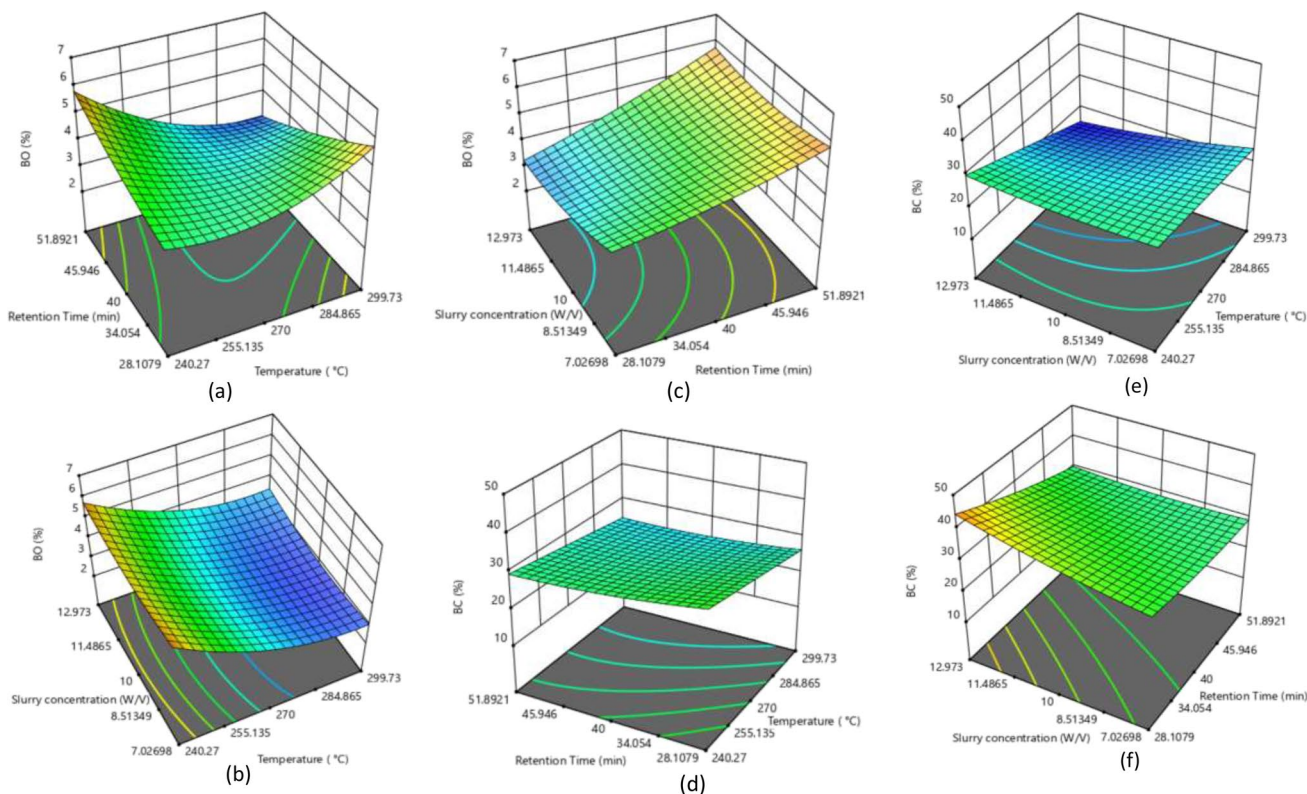

Fig. 1 The 3D response surface curve showing the effect of independent variables, i.e., temperature (240 °C), retention time (52 min), and slurry concentration (7% w/v) on BO (**a**, **b**, and **c**) and BC (**d**, **e**, and **f**)

Figure 2 (a) and (b) illustrate the normal probability plot used to assess the model's suitability. Most of the experimental data for each response are often linear, and the model error is explained by the interval between the point's location and the line. When the residual value does not reflect the normal distribution, the cumulative distribution for a certain population may be calculated using residuals that would nearly follow a straight line (Eloy et al. 2020). The errors are regularly distributed based on normal distribution plots, and the underlying assumptions of the inquiry have practically never been neglected (Wu et al. 2012; Hassan et al. 2019).

Optimization using the desirability function

Numerical optimization of independent variables (temperature, retention time, and slurry concentration) was carried out by using the software Design-Expert 13.0.1. As part of the investigation's objectives, the goal was set for all independent variables. The responses, BO production, and BC yield were considered for optimization.

The model was analyzed separately to select the optimum conditions and range. The optimization was carried out in accordance with the criteria shown in Fig. 3. During optimization, a total of 72 solutions were generated, with the one that best fitting the benchmark in terms of desirability being chosen.

The optimized values of HTL process parameters were found to be 240 °C (temperature), 52 min (retention time), and 7% (slurry concentration) and the corresponding responses were 5.794% BO yield and 29.450% BC yield. Experiments at optimum conditions were performed, and

Table 4 Predicted and experimental values of HTL process based on numerical optimization

Parameters	Predicted	Experimental
Temperature (°C)	240	240
Retention time (min)	52	52
Slurry concentration (%) (solid to solvent ratio)	7	7
BO yield (%)	5.794 ± 0.116	5.932 ± 0.091
BC yield (%)	29.450 ± 0.086	30.140 ± 0.134

the results were analyzed to validate the optimized values. Table 4 shows the good agreement between the anticipated values and the experimental outcome.

Instrumental analysis of product

FT-IR analysis of CPP and BC

The FT-IR spectra of CPP and obtained BC through the HTL process are shown in Fig. 4 and Table 5. The FT-IR spectra identify the functional group present in CPP and obtain bio-chars. The peak at 3435 cm^{-1} in CPP spectra reveals the stretching vibrations of O–H while C=O stretching vibrations occur at 1742 cm^{-1}. Both the O–H and C=O stretching vibrations verify the −COOH group (Huff and Lee 2016). Peaks at 2935 cm^{-1} correlate to stronger C–H stretching from methylene and methyl groups due to the CPP's higher fatty acid content. The
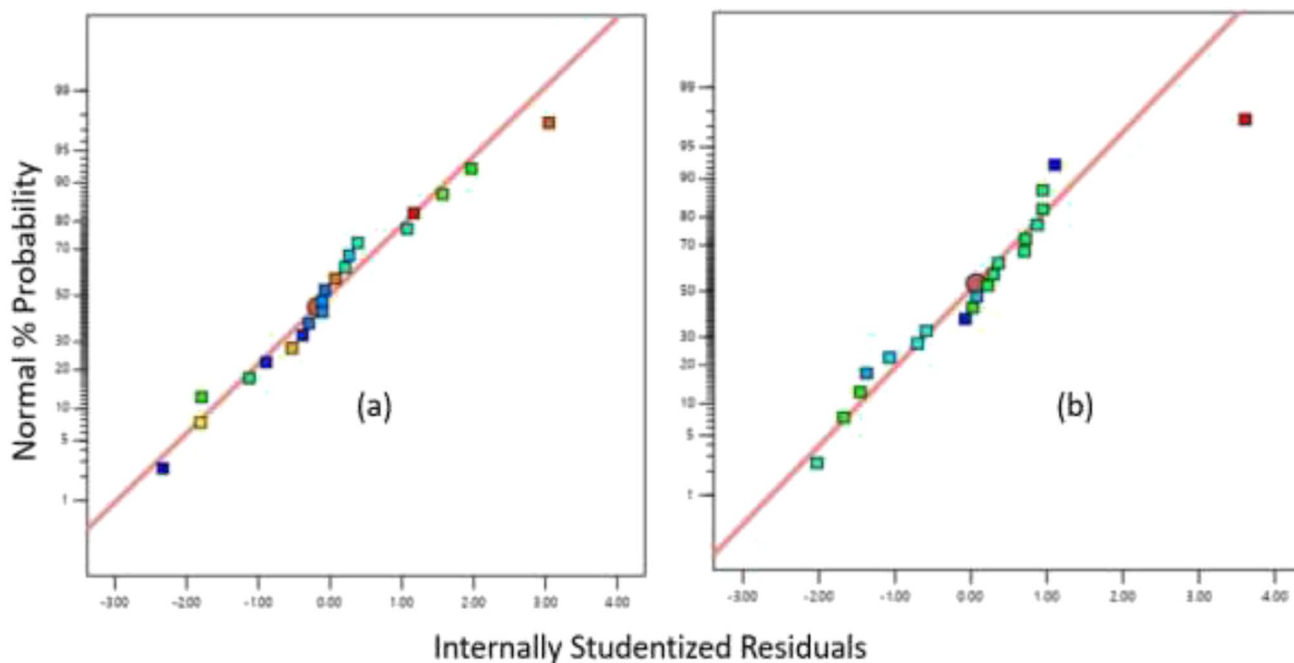

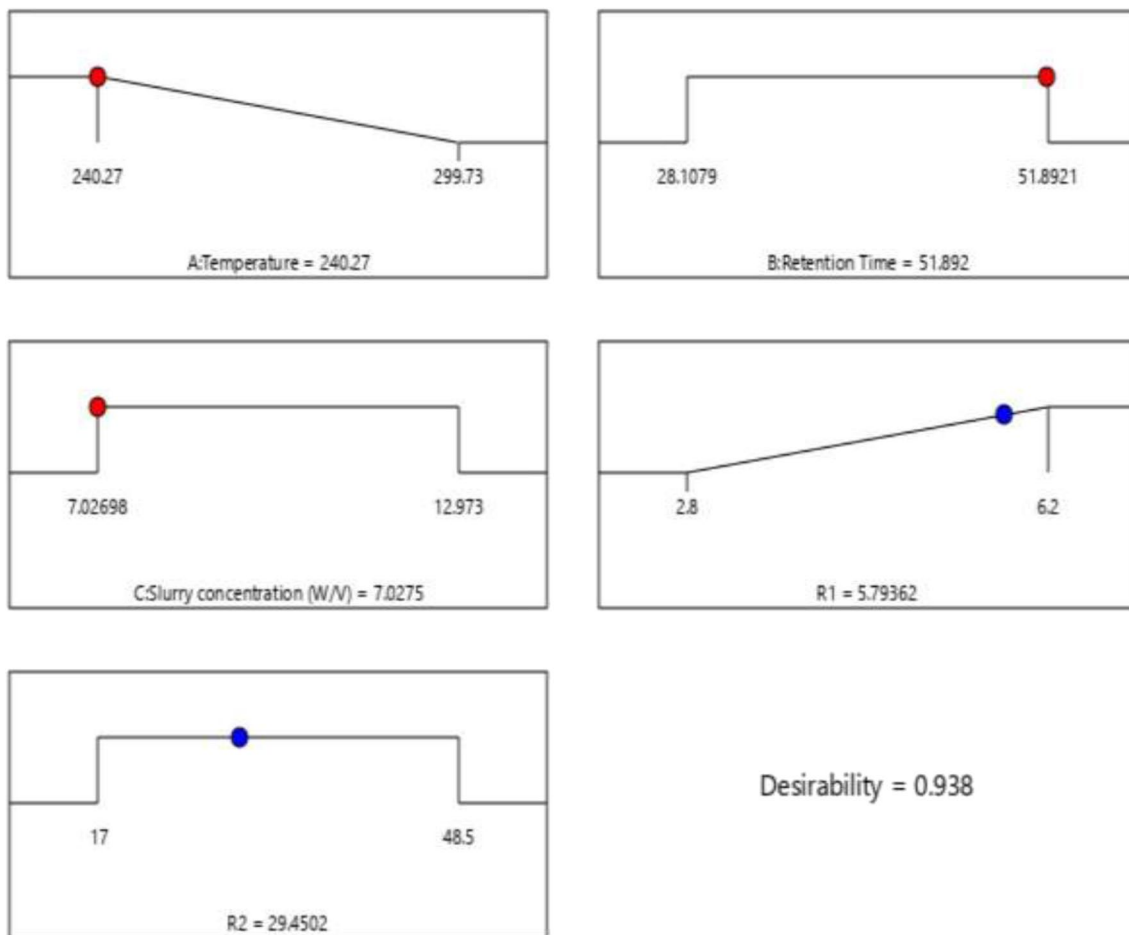**Fig. 2** Standard normal probability plot of BO yield (**a**) and BC (**b**)

Fig. 3 Desirability ramp of HTL process parameters

reduction in absorption peak at 2925 cm^{-1} in bio-chars corresponds to the stretching vibrations of the C–H band of cellulose and hemicellulose, and the removal of a methyl group decreases the intensity of O–H groups from 3435 to 3432 cm^{-1} and exhibits the decomposition of phenolic functionalities (Mullen and Boateng 2008). In the study of the BC spectra, the decreasing intensity of the carboxylic group is observed due to the CPP volatilization in the HTL process.

The H-NMR spectra of the optimized BO (240 °C, 52 min, 7% slurry concentration) are shown in Fig. 5. The spectra indicated a general variation in the chemical compositions of the BO. The most upfield spectra, from 0.9 to 1.5 ppm of BO, stipulate the aliphatic − H that are joined with carbon molecules. A minimum of two bonds removed from C = C or heteroatom (O or N) indicates the aliphatic substances for BO (Mullen et al. 2009).

Similarly, in the next region from 1.5 to 2.5 ppm, notable protons joined on aliphatic carbon atoms that may be
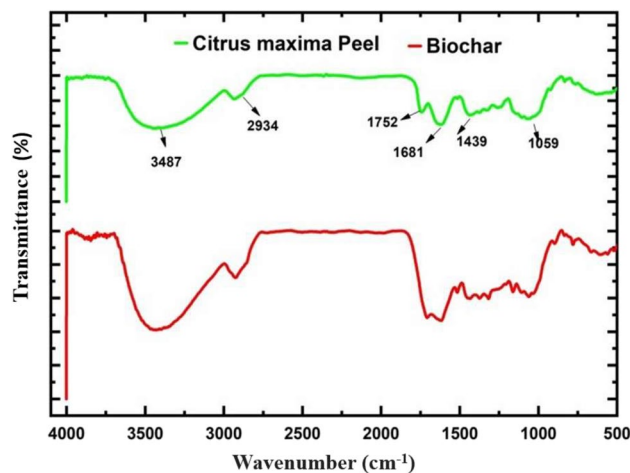
Fig. 4 FT-IR study of CPP and HTL obtained bio-char

bonded to a C = C (aromatic or olefinic) (Fig. 5). These spectra have shown rich protons in this region and put forward,

Table 5 FT-IR spectral band of CPP and BC with functional group

Wave numbers (cm^{-1})	Assignments	CPP	BC
3700–3200	O–H stretching acid, methanol	3435.8	3432.4
3000–2800	C–H$_n$ stretching, alkyl, aliphatic, aromatic	2935.3	2925.7
1750–1630	C=O stretching, ketone, ester, amide	1742.2	-
1640–1535	C=O groups	1619.2	1619.1
1440–1400	OH, bending acid	1438.1	1434.6
1300–1100	C–O stretching	1257.4	-
1340–1250	C–N stretching	-	1317.2
1070–1050	CH$_2$ twisting	1062.4	1061.0
700–400	C–C stretching	632.1	606.5

^{1}H-NMR analysis of BO

the aliphatic part, aromatic part, or close heteroatoms of molecules are presiding for containing higher energy BO (Boateng et al. 2007).

The downfield spectrum region from 2.5 to 4.5 ppm represents protons on carbon atoms next to an aliphatic alcohol or ether or a methylene group that attached two aromatic rings. The region between 4.5 and 6.5 ppm represents aromatic ether protons, and many carbohydrate-like molecules' hydrogen atoms. The spectrum region 6.5–8.0 ppm indicates hydrogen atoms in benzenoids and those in heteroaromatics containing O and N (Mullen and Boateng 2008).

GC–MS analysis of bio-oil

Chemical compositions of the optimized BO (240 °C, 52 min, 7% slurry concentration) were obtained using GC–MS at 300 °C, 60 min, and the spectra are shown in Table 6. Total area is 97.59% only science; there are unidentified peaks less than 1% area. BO mainly comprises cyclic oxygenates (phenol derivatives, etc.), organic acids (fatty acids), alcohols, hydrocarbons, and esters. BO composition depends upon feedstock and operational conditions. GC–MS spectra display the long-chain fatty acid and its derivatives, which are formed via hydrolysis
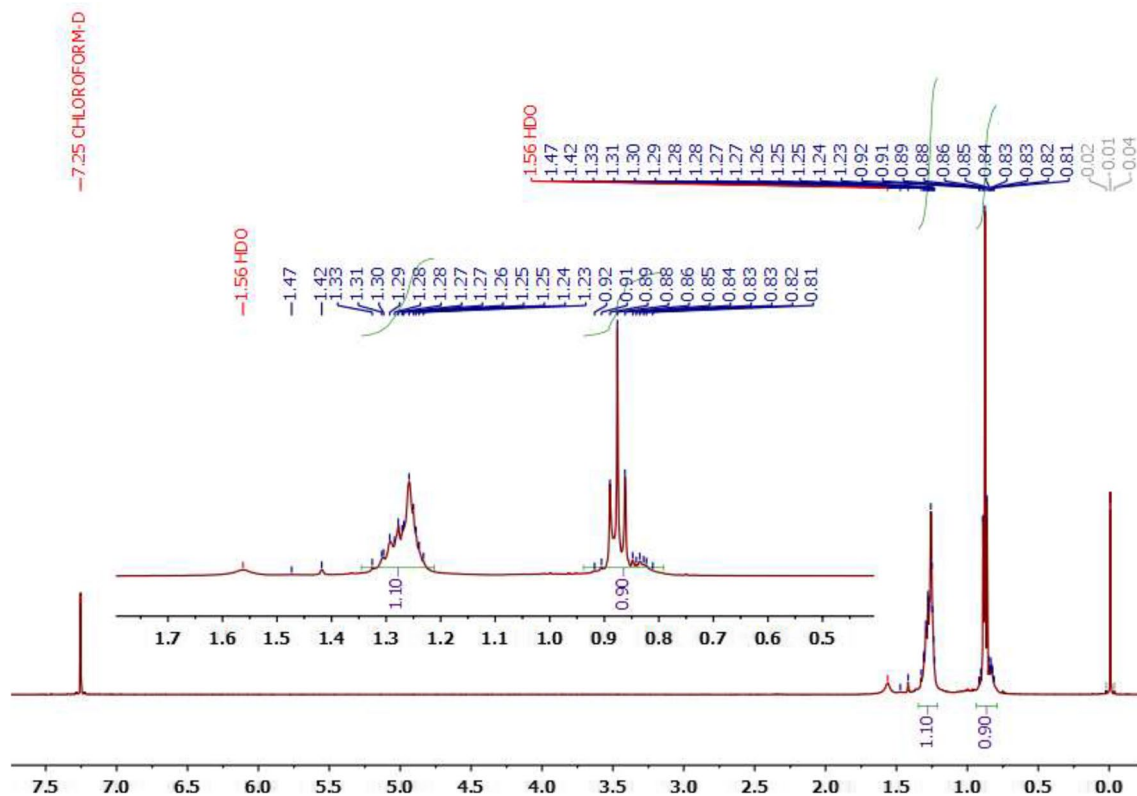

Fig. 5 The ^{1}H NMR spectra of BO obtained from HTL of *Citrus maxima* peel

Table 6 Major compounds identified by GC–MS in BO of CPP

Compound name	Molecular weight	Category	Area (%)
Octane, 3,5-dimethyl-	142	Hydrocarbon alkane	7.32
Eugenol	164	Essential oils	4.89
Pentanedioic acid, (2,4-di-T-butylphenyl)	320	Mono-ester	13.54
N-hexadecanoic acid	256	Fatty acid	20.13
Tetracosanoic acid	368	Fatty acid	2.05
Eicosanoic acid	312	Fatty acid	6.32
Docosanoic acid	340	Fatty acid	3.57
Cholesteryl phenylacetate	504	Esters	1.14
Octadecane	254	Alkane hydrocarbon	2.13
Octanoic acid, 6-ethyl-3-octyl ester	284	Fatty acid	1.98
Eicosyl heptyl ether	396	Ether	9.68
Stigmasterol	412	Fatty acid	16.08
Hexacosyl nonyl ether	508	Fatty acid	8.76

of lipids in HTL such as cholesteryl phenylacetate, eicosanoic acid, octanoic acid, and 6-ethyl-3-octyl ester. It can be seen that presence of phenolic derivatives was obtained due to the presence of carbohydrates (Gai et al. 2015; Arturi et al. 2017).

Future prospects

BO produced via HTL of lignocellulose biomass still had significant limitations such as poor yields and high oxygen content, which led to numerous operational issues, such as corrosion, instability, and decreased HHV. As a result, improving the stability and HHV of BO produced by the HTL method has remained crucial. Catalytic HTL is presently the cutting-edge and cost-effective technique for improving the stability and quality of BO. For example, catalytic HTL with citric acid surfactants/solid catalysts enhanced the conversion of *Citrus maxima* peel to BO with a greater yield (26.10–67.72 wt%) at low temperatures (200 °C) (Wei et al. 2023). Similarly, at the same temperature, the same peel waste was investigated with a different catalyst (ionic liquid loaded ZSM-5) with remarkable BO production of 19.68 wt% (Wei et al. 2022).

Conclusion

The current study was focused on the potential utilization of *Citrus maxima* peel waste to produce BO and BC through the HTL process. Experimental design and optimization were performed using Design-Expert software 13.0.1, RSM-CCD model. According to the study findings, the following conclusion is drawn: 5.932% BO and 30.14% BC were obtained at optimum conditions via the HTL process. FT-IR spectra evidence the presence of the carboxylic group in CPP. While the intensity of the carboxylic group decreases due to reaction time and temperature. Aliphatic protons predominate in bio-oils produced by the HTL process, while protons near to heteroatoms (carbohydrates and alcohol) are particularly intense in ^{1}H-NMR. According to GC–MS analysis, BO has many long-chain fatty acids. As a result, this study can be used to design and apply laboratory-scale system for utilization of *Citrus maxima* peel waste.

Data availability All data generated or analyzed during this study are included in this published article and its supplementary information files.

Declarations

Ethical approval and consent to participate Not applicable.

Consent for publication Not applicable.

Competing interests The authors declare no competing interests.

References

Acharya S, Kishore N (2022) *Citrus limetta* fruit waste management by liquefaction using hydrogen-donor solvent. RSC Adv 12:32708–32721. https://doi.org/10.1039/D2RA06085J

ÁngelSilesLópez J, Li Q, Thompson IP (2010) Biorefinery of waste orange peel. Crit Rev Biotechnol 30:63–69. https://doi.org/10.3109/07388550903425201

Arora N, Jaiswal KK, Kumar V, Vlaskin MS, Nanda M, Pruthi V, Chauhan PK (2020) Small-scale phyco-mitigation of raw urban wastewater integrated with biodiesel production and its utilization for aquaculture. Bioresour Technol 297:122489. https://doi.org/10.1016/j.biortech.2019.122489

Arturi KR, Strandgaard M, Nielsen RP, Søgaard EG, Maschietti M (2017) Hydrothermal liquefaction of lignin in near-critical water in a new batch reactor: influence of phenol and temperature. J Supercrit Fluids 123:28–39. https://doi.org/10.1016/j.supflu.2016.12.015

Boateng AA, Daugaard DE, Goldberg NM, Hicks KB (2007) Bench-scale fluidized-bed pyrolysis of switchgrass for bio oil production. Ind Eng Chem Res 46:1891–1897. https://doi.org/10.1021/ie0614529

Changi SM, Faeth JL, Mo N, Savage PE (2015) Hydrothermal reactions of biomolecules relevant for microalgae liquefaction. Ind Eng Chem Res 54:11733–11758. https://doi.org/10.1021/acs.iecr.5b02771

Chen X, Xu X, Lu Z, Zhang W, Yang J, Hou Y, Wang X, Zhou S, Li Y, Wu L, Zhang F (2020) Carbon footprint of a typical pomelo production region in China based on farm survey data. J Clean Prod 277:124041. https://doi.org/10.1016/j.jclepro.2020.124041

Chen WH, Lin YY, Liu HC, Baroutian S (2020) Optimization of food waste hydrothermal liquefaction by a two-step process in association with a double analysis. Energy 199:117438. https://doi.org/10.1016/j.energy.2020.117438

Divyabharathi R, Subramanian P (2022) Biocrude production from orange (*Citrus reticulata*) peel by hydrothermal liquefaction and process optimization. Biomass Convers Biorefin 12:183–194. https://doi.org/10.1007/s13399-021-01383-3

Eloy JO, Ruiz A, de Lima FT, Petrilli R, Raspantini G, Nogueira KAB, Santos E, de Oliveira CS, Borges JC, Marchetti JM, Al-Jamal WT, Chorilli M (2020) EGFR-targeted immunoliposomes efficiently deliver docetaxel to prostate cancer cells. Colloids Surf B Biointerfaces 194:111185. https://doi.org/10.1016/j.colsurfb.2020.111185

Gai C, Zhang Y, Chen WT, Zhang P, Dong Y (2015) An investigation of reaction pathways of hydrothermal liquefaction using *Chlorella pyrenoidosa* and *Spirulina platensis*. Energy Convers Manag 96:330–339. https://doi.org/10.1016/j.enconman.2015.02.056

Gururani P, Bhatnagar P, Bisht B, Jaiswal KK, Kumar V, Kumar S, Vlaskin MS, Grigorenko AV, Rindin KG (2022) Recent advances and viability in sustainable thermochemical conversion of sludge to bio-fuel production. Fuel 316:123351. https://doi.org/10.1016/j.fuel.2022.123351

Hassan MZ, Sapuan SM, Roslan SA, Sarip S (2019) Optimization of tensile behavior of banana pseudo-stem (*Musa acuminate*) fiber reinforced epoxy composites using response surface methodology. J Mater Res Technol 8:3517–3528. https://doi.org/10.1016/j.jmrt.2019.06.026

Huang R, Cao M, Guo H, Qi W, Su R, He Z (2014) Enhanced ethanol production from pomelo peel waste by integrated hydrothermal treatment, multienzyme formulation, and fed-batch operation. J Agric Food Chem 62:4643–4651. https://doi.org/10.1021/jf405172a

Huff MD, Lee JW (2016) Biochar-surface oxygenation with hydrogen peroxide. J Environ Manage 165:17–21. https://doi.org/10.1016/j.jenvman.2015.08.046

Jiang J, Savage PE (2017) Influence of process conditions and interventions on metals content in biocrude from hydrothermal liquefaction of microalgae. Algal Res 26:131–134. https://doi.org/10.1016/j.algal.2017.07.012

Khuri AI, Cornell JA (1987) Response surface design and analysis. Marcel Skker, Inc. ASQC Quality Press, New Delhi, pp 112–139

Kumar M, Oyedun AO, Kumar A (2018) A review on the current status of various hydrothermal technologies on biomass feedstock. Renew Sust Energ Rev 81:1742–1770. https://doi.org/10.1016/j.rser.2017.05.270

Kumar S, Kaur G, Joshi A, Joshi HC (2019a) Production of biodiesel from *Citrus maxima* (Chakotara) seed oil, a potential of non-food feedstock and its blends with n butanol-diesel and purification, utilization of glycerol obtained as by-product from biodiesel. Energy Sources A Recover Util Environ Eff 41:1508–1517. https://doi.org/10.1080/15567036.2018.1549125

Kumar V, Kumar S, Chauhan PK, Verma M, Bahuguna V, Joshi HC, Ahmad W, Negi P, Sharma N, Ramola B, Rautela I, Nanda M, Vlaskin MS (2019b) Low-temperature catalyst based hydrothermal liquefaction of harmful macroalgal blooms, and aqueous phase nutrient recycling by microalgae. Sci Rep 9:1–9. https://doi.org/10.1038/s41598-019-47664-w

Li Z, Cao J, Huang K, Hong Y, Li C, Zhou X, Xie N, Lai F, Shen F, Chen C (2015) Alkaline pretreatment and the synergic effect of water and tetralin enhances the liquefaction efficiency of bagasse. Bioresour Technol 177:159–168. https://doi.org/10.1016/j.biortech.2014.11.043

Long J, Li Y, Zhang X, Tang L, Song C, Wang F (2016) Comparative investigation on hydrothermal and alkali catalytic liquefaction of bagasse: process efficiency and product properties. Fuel 186:685–693. https://doi.org/10.1016/j.fuel.2016.09.016

Mazaheri H, Lee KT, Mohamed AR (2013) Influence of temperature on liquid products yield of oil palm shell via subcritical water liquefaction in the presence of alkali catalyst. Fuel Process Technol 110:197–205. https://doi.org/10.1016/j.fuproc.2012.12.015

Methacanon P, Krongsin J, Gamonpilas C (2014) Pomelo (*Citrus maxima*) pectin: effects of extraction parameters and its properties. Food Hydrocoll 35:383–391. https://doi.org/10.1016/j.foodhyd.2013.06.018

Mullen CA, Boateng AA (2008) Chemical composition of bio-oils produced by fast pyrolysis of two energy crops. Energy Fuels 22(3):2104–2109. https://doi.org/10.1021/ef700776w

Mullen CA, Strahan GD, Boateng AA (2009) Characterization of various fast-pyrolysis bio-oils by NMR spectroscopy. Energy Fuels 23:2707–2718. https://doi.org/10.1021/ef801048b

Naruka M, Khadka M, Upadhayay S, Kumar S (2019) Potential applications of microalgae in bioproduct production: a review. Octa J Biosci 7:01–05

Pourbafrani M, McKechnie J, MacLean HL, Saville BA (2013) Life cycle greenhouse gas impacts of ethanol, biomethane and limonene production from citrus waste. Environ Res Lett 8:015007. https://doi.org/10.1088/1748-9326/8/1/015007

Sadhukhan B, Mondal NK, Chattoraj S (2016) Optimisation using central composite design (CCD) and the desirability function for sorption of methylene blue from aqueous solution onto *Lemna major*. Karbala Int J Mod Sci 2:145–155. https://doi.org/10.1016/j.kijoms.2016.03.005

Shafiee S, Topal E (2009) When will fossil fuel reserves be diminished? Energy Policy 37:181–189. https://doi.org/10.1016/j.enpol.2008.08.016

Ting SV, Deszyck EJ (1961) The carbohydrates in the peel of oranges and grapefruit a. J Food Sci 26:146–152. https://doi.org/10.1111/j.1365-2621.1961.tb00784.x

Tocmo R, Pena-Fronteras J, Calumba KF, Mendoza M, Johnson JJ (2020) Valorization of pomelo (*Citrus grandis* Osbeck) peel: a review of current utilization, phytochemistry, bioactivities, and mechanisms of action. Compr Rev Food Sci Food Saf 19:1969–2012. https://doi.org/10.1111/1541-4337.12561

Wei Y, Fakudze S, Zhang Y, Song M, Xue T, Xie R, Chen J (2022) Low-temperature hydrothermal liquefaction of pomelo peel for

production of 5-hydroxymethylfurfural-rich bio-oil using ionic liquid loaded ZSM-5. Bioresour Technol 352:127050. https://doi.org/10.1016/j.biortech.2022.127050

Wei Y, Fakudze S, Yang S, Zhang Y, Xue T, Han J, Chen J (2023) Synergistic citric acid-surfactant catalyzed hydrothermal liquefaction of pomelo peel for production of hydrocarbon-rich bio-oil. Sci Total Environ 857:159235. https://doi.org/10.1016/j.scitotenv.2022.159235

Wu L, Yick KL, Ng SP, Yip J (2012) Application of the Box-Behnken design to the optimization of process parameters in foam cup molding. Expert Syst Appl 39:8059–8065. https://doi.org/10.1016/j.eswa.2012.01.137

Xue J, Grift TE, Hansen AC (2011) Effect of biodiesel on engine performances and emissions. Renew Sust Energ Rev 15:1098–1116. https://doi.org/10.1016/j.rser.2010.11.016

Zhang B, Chen J, He Z, Chen H, Kandasamy S (2019) Hydrothermal liquefaction of fresh lemon-peel: parameter optimisation and product chemistry. Renew Energ 143:512–519. https://doi.org/10.1016/j.renene.2019.05.003